

University of Mississippi

eGrove

Honors Theses

Honors College (Sally McDonnell Barksdale
Honors College)

Spring 5-4-2022

Computational and Spectroscopic Studies of New Sulfur-Containing Dipole-Bound Anions

Nicholas Allen Kruse
University of Mississippi

Follow this and additional works at: https://egrove.olemiss.edu/hon_thesis

 Part of the [Computational Chemistry Commons](#), and the [Physical Chemistry Commons](#)

Recommended Citation

Kruse, Nicholas Allen, "Computational and Spectroscopic Studies of New Sulfur-Containing Dipole-Bound Anions" (2022). *Honors Theses*. 2620.

https://egrove.olemiss.edu/hon_thesis/2620

This Undergraduate Thesis is brought to you for free and open access by the Honors College (Sally McDonnell Barksdale Honors College) at eGrove. It has been accepted for inclusion in Honors Theses by an authorized administrator of eGrove. For more information, please contact egrove@olemiss.edu.

Computational and Spectroscopic Studies of New Sulfur-Containing Dipole-Bound Anions

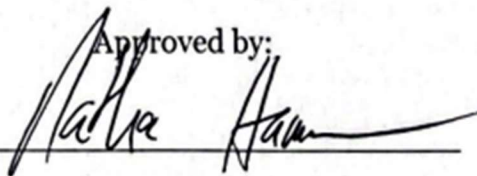
By Nicholas A. Kruse

A thesis submitted to the faculty of the University of Mississippi in partial fulfillment of the requirements of the Sally McDonnell Barksdale Honors College

Oxford

April 2022

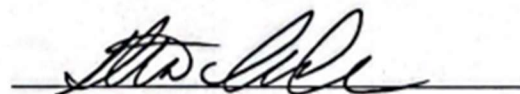
Approved by:

A handwritten signature in black ink, appearing to read "Nathan Hammer", written over a horizontal line.

Dr. Nathan I. Hammer (Advisor)

A handwritten signature in black ink, appearing to read "Ryan Fortenberry", written over a horizontal line.

Dr. Ryan C. Fortenberry (Reader)

A handwritten signature in black ink, appearing to read "Steven R. Davis", written over a horizontal line.

Dr. Steven R. Davis (Reader)

Copyright © 2022
Nicholas A. Kruse
ALL RIGHTS RESERVED

Acknowledgements

To my family, words cannot express the gratitude I have towards you all. From that first piano lesson to my acid-base project at the middle school science fair and beyond, thank you for your immeasurable support and care. To Trevor Wolfe, Sebastian Mink, and Johnny Bethea, you three have been ultimate trio of friends I could always count on. From helping me with research struggles to listening to my endless stream of stories, you three have never let me down and are the best friends I could have asked for. To the Hammer Lab & Friends, namely Dr. Ashley Williams, Dr. Leigh Anna “KQ” Hunt, Dr. Austin Dorris, Dr. April Hardin, Dr. Shane Autry, Ethan Lambert, and Seth Darlington, thank you all for the incredible help from the moment I set foot in the lab as a wide-eyed freshman. For the lessons learned and the laughs shared, thank you all so much. To the Ole Miss Physics Department, namely Dr. Labuda, thank you for the financial resources and incredible instruction over the past four years. To Dr. Ryan Fortenberry, thank you for being an incredible professor and for showing me how to share my love of chemistry with the rest of the world. Finally, to the greatest mentor I’ve ever had, Dr. Nathan Hammer, I would not be the man, researcher, and TA I am today without you. Your guidance over the past four years has been more impactful than I could have ever imagined, and I cannot wait to spend the next stage of my life working for you as a graduate student. To quote one of my favorite Shinedown songs, “you [all] are the miracle in me,” and I will be eternally grateful for the impact you all have had on me.

Abstract

Sulfur and Nitrogen are essential ingredients in both life-supporting and light-harvesting molecules. Their presence also usually leads to the delocalization of electrons and large dipole and quadrupole moments. Such molecules are sometimes able to form negative ions through the electrostatic binding of an excess electron. These so-called multipole-bound (dipole-bound, quadrupole-bound, etc.) anions have been shown to be important in radiation damage in biology and electron transport processes. Here, we present our recent computational and experimental results studying the creation of new multipole-bound anions.

Table of Contents

Title	1
Acknowledgements	3
Abstract	4
Table of Contents	5
List of Figures	6
List of Tables	7
Chapter I: Introduction to Dipole-Bound Anions.....	8
Chapter II: Mass Spectrometry and Vacuum Technology	13
Section I: Time-of-Flight Mass Spectrometry	13
Section II: Vacuum Technology	16
Chapter III: Experimental Methods.....	20
Chapter IV: Computational Chemistry	26
Section I: Introduction to Quantum Chemistry	26
Section II: Computational Methods.....	29
Chapter V: Results	33
Chapter VI: Conclusions and Future Work.....	39
References.....	41

List of Figures

Figure 1.1: Electron Affinity as depicted by the overlapping of Morse Potentials.....	10
Figure 2.1: Original Wiley-McLaren TOFMS Schematic.....	14
Figure 2.2: Schematic showcasing the basics of the Reflectron.....	15
Figure 2.3: Rotary Vane Roughing Pump.....	17
Figure 2.4: Turbomolecular Pump	19
Figure 3.1: Schematic of Experimental Setup.....	20
Figure 3.2: Time-of-Flight Mass Spectrometer	22
Figure 3.3: Micro-Channel Plate Detector.....	23
Figure 3.4: Z-Stack Mounted Micro-Channel Plate Detector	24
Figure 5.1: Comparison of Dipole Moments and Electron Affinities of New Molecules with Previously-Studied Molecules	35
Figure 5.2: Optimized Lowest Unoccupied Molecular Orbitals.....	36

List of Tables

Table 5.1.....	34
----------------	----

Chapter I

Introduction to Dipole-Bound Anions

Electron transport processes are a fundamental topic in chemistry and are critical to understanding both the specifics of chemical reactions and the world in general. Moreover, they play a crucial role in energy transference, spectroscopy, and, in the case of this project, light harvesting. It is believed that by studying fundamental electron-transport processes, solar energy harvesting devices known as dye-sensitized solar cells (DSCs) can be better understood and optimized. In a dye-sensitized solar cell, the modern form of which was invented in 1991¹, a dye, anchored to the surface of a titanium dioxide semiconductor, absorbs photons and subsequently injects them into the semiconductor. These electrons then pass through an external circuit, are retrieved via a redox shuttle, and are finally returned to the newly-oxidized dye to regenerate what is known as a ground-state photosensitizer² – a photoactive molecule that absorbs light energy to catalyze reactive oxygen species formation³. As of 2010, the best DSC had a maximum efficiency of only 13.4%⁴. Even in recent studies performed by the Delcamp and Hammer Research Groups at the University of Mississippi, the vast majority of devices had power conversion efficiencies (PCEs) in the range of 5-8%⁵⁻⁸. Even for other forms of solar cells, the highest efficiency found in commercially available solar cells is only 22%⁹. This low efficiency in combination with the high cost of production, distribution, and installation is most likely the cause for the lack of

widespread solar cell use. To combat this, a better understanding of the inner workings of solar cells, specifically DSCs for the course of this project, was sought. However rather than looking forward to completely new fields, it was found that the answers sought could possibly be found by a trip to the past.

Nearly two decades ago, Dr. Nathan Hammer, under the advisement of Dr. Robert Compton, began creating and studying the properties of what are known as dipole-bound anions, or DBAs. Now, anions, or negative ions, are atoms or molecules that possess a net negative charge. The vast majority of elements on the periodic table *can* form a negative ion, however some are more likely than others to do so. Atoms or molecules with a positive electron affinity are known to form such ions. Electron affinity has been defined as the difference in energy between the ground state of the neutral atom or molecule and the ground state of its anionic counterpart. For a dipole-bound anion, the graphical representation of electron affinity is depicted as such:

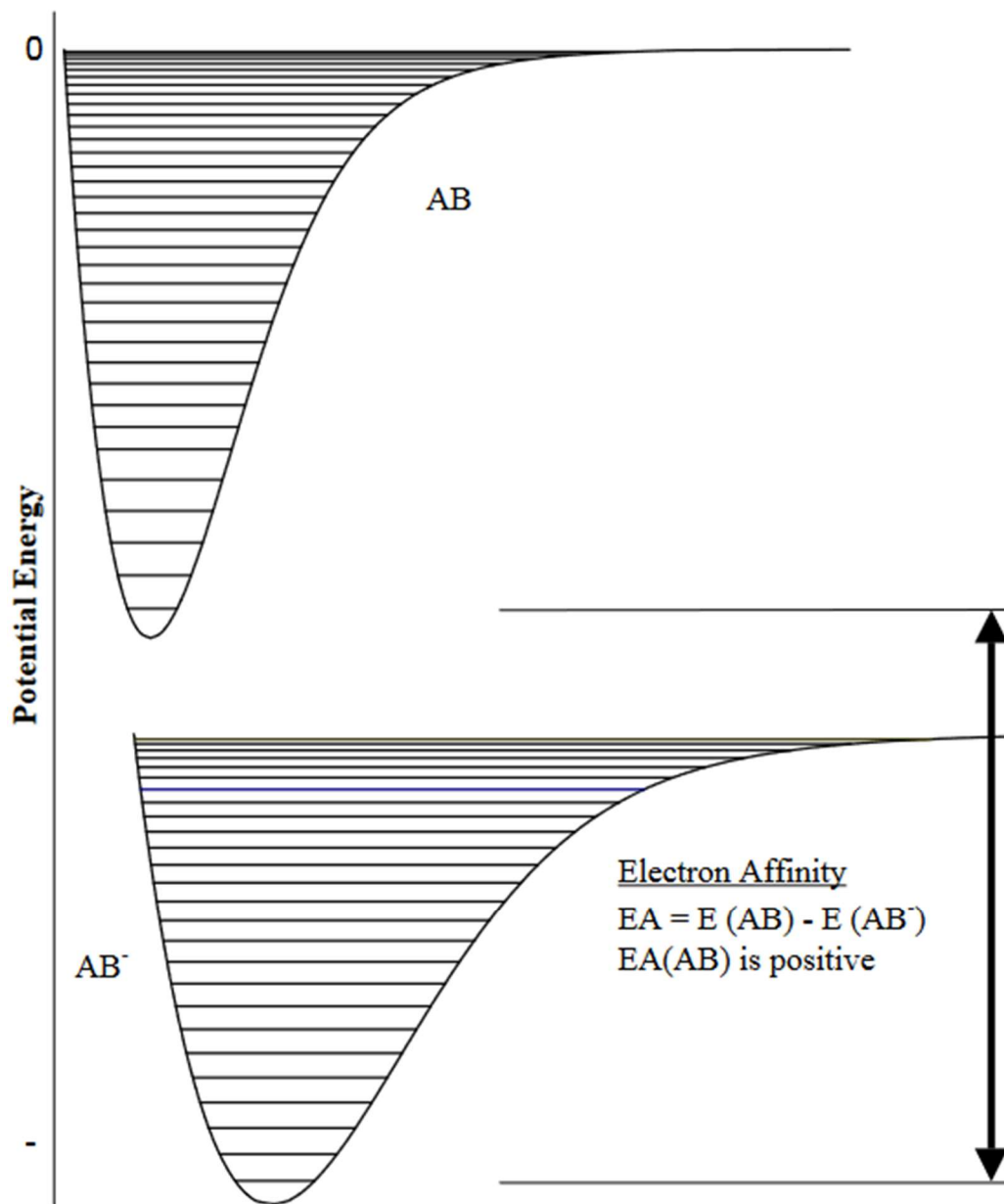


Figure 1.1: Electron Affinity as depicted by the overlapping of Morse Potentials¹⁰

Both curves are the graphical representations of electronic energy levels, dubbed Morse Potentials. The Morse Potential was first proposed by Phillip M. morse in 1929 as a better description of rovibronic energy levels

as compared to the simple harmonic oscillator beloved by physicists¹¹. As can be seen in Figure 1.1, the potential energy diagram of the anion is less than that of the neutral ion, meaning the anionic state is not only achievable, but favored, as a positive electron affinity indicates that the binding of an electron is a spontaneous reaction. Moreover, the higher the electron affinity, the more stable the anionic state. For atomic anions, it is widely known that chloride is the most stable, however for molecular anions, which have been critically understudied, data is much scarcer. Thus, Dr. Hammer began computational and experimental studies on such molecules, producing seven publications and a dissertation on the project^{10,12-15}.

The first recorded study on dipole-bound states was performed in 1947 by Enrico Fermi and Edward Teller, where they found that the minimum dipole moment to bind an electron via what they named a “point dipole” was 1.625 Debye^{10,16}. It was later found by Wallis et. Al. in 1960 that below ~2.5 Debye, the binding energy (or electron affinity) was extremely small (<1 meV), however at higher dipole moments, this value drastically increased^{10,17}. In the decades following these initial studies proving the existence of such an anion, many a computational study has been performed attempting to understand them as well as photoelectron spectroscopic studies¹⁸. After the work performed by Dr. Hammer and Dr. Compton, the field began to gain a small amount of traction, however no significant advances in the experimental side of the field have been made.

Thus, three years ago, this “sequel” project began. It began with a computational study, the results of which are presented here, which was designed to predict which molecules would be best suited for experimental study. It was known at the beginning of the project that molecules with an extremely high dipole moment, preferably above 2.5 Debye¹⁷, are the best candidates for experimental study, however not every molecule with a dipole moment above 2.5 Debye has a dipole-bound anionic state. Thus, this could only be an initial filter for potential experimental candidates. Following this selection, computational chemical methods were utilized to further narrow down this list of molecules to those with a positive electron affinity as both determined by subtracting the zero-point energy of the neutral molecule from that of the anion and also from the application of Koopman’s Theorem, which tells us that the electron affinity of a molecule is equivalent to the energy of its lowest unoccupied molecular orbital. This method resulted in the selection of six molecules: 1,3-dioxolan-2-thione, 1,3-dioxole-2-thione, ethylene-thiocarbonate, vinylene-thiocarbonate, furfural, and 1,3,4-thiadiazole. These six molecules, all with dipole moments above 3 Debye, proved to be especially interesting candidates for experimental study, as well as their “variants,” or molecules chemically similar in nature but with alterations both intriguing and relatively simple to synthesize.

Chapter II

Mass Spectrometry and Vacuum Technology

Section I: Time-of-Flight Mass Spectrometry

To analyze this unique class of anions, both computational and spectroscopic techniques were utilized. The computational methods are described in Chapter IV, however to perform laboratory analysis, a technique known as Time-of-Flight Mass Spectrometry was used. Time-of-Flight Mass Spectrometry (TOFMS) is an extremely effective method for analyzing the mass-to-charge ratio of molecules in an effort to determine their identities. Operating on the basic principles of electromagnetism and simple mechanics, TOFMS measures the time required for the particles under study to travel through the flight tube and hit the detector (hence the name, “time-of-flight.”). Though the principles of flight time with regards to electromagnetic effects have been known since the days of J.J. Thomson, the first Time-of-Flight Mass Spectrometer wasn’t proposed until W. E. Stephens did so in the late 1940’s and wasn’t experimentally tested until Cameron and Eggers did so in 1948. Even then, a commercial version of the instrument wasn’t released until 1955 when Katzenstein and Friedland found that the key to optimizing the procedure was the pulsation of the ion source and Wiley and McLaren designed the first commercially successful Time-of-Flight Mass Spectrometer, depicted below¹⁹:

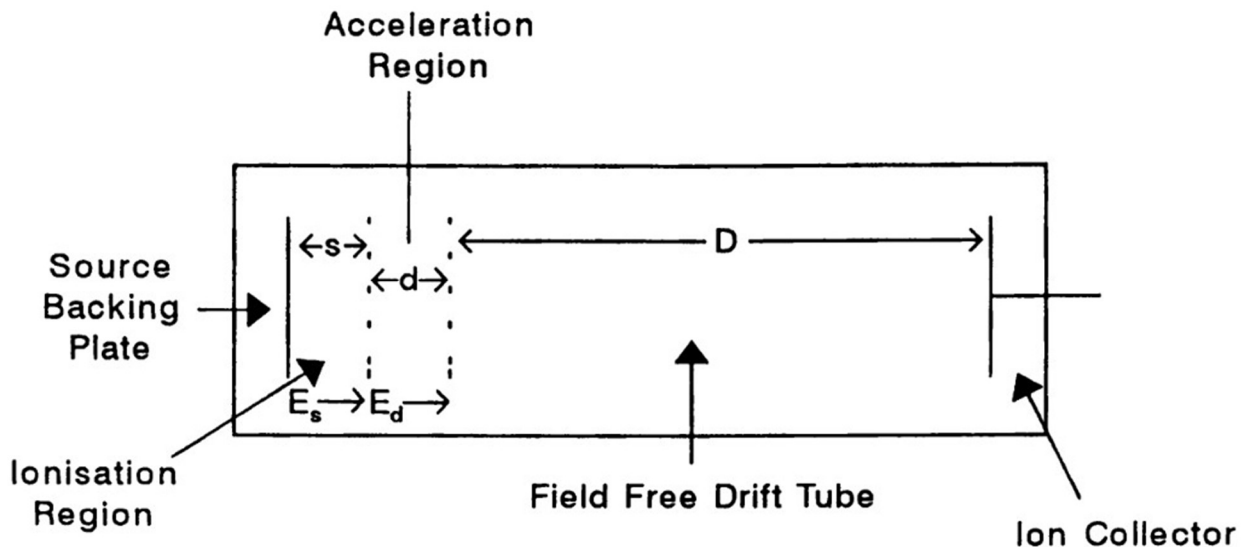


Figure 2.1: Original Wiley-McLaren TOFMS Schematic¹⁹

Initial designs didn't account for the spatial distribution of the molecules upon ionization or initial kinetic energy distribution, which created a range of times in which ions of the same mass-to-charge ratio reach the detector, making it difficult to distinguish between ions. However, Wiley and McLaren accounted for this by creating a two-grid ion source with dimensions optimized to account for these discrepancies.¹⁹

Since this first commercial time-of-flight mass spectrometer, which admittedly didn't have the highest resolution, many more versions of and improvements on the instrument have been made. In the second European Time-of-Flight Mass Spectrometry Symposium in 1969, a new series of time-of-flight mass spectrometry, entitled Dynamic Mass Spectrometry, was introduced. Additionally, it was around this time period in which mass spectrometry found its use as a detector for other analytical techniques.

time-of-flight mass spectrometry, given its incredibly quick scanning capability, turned out to be a perfect fit as a detector for gas chromatography, leading to the development of Gas Chromatography/Mass Spectrometry, or GC/MS, a technique still widely utilized today¹⁹.

Since these early days of time-of-flight mass spectrometry, many new techniques and applications have been designed, such as various surface analysis techniques including Secondary Ion Mass Spectrometry (SIMS) and the Reflectron, which alters the paths of the anions using a series of different voltages, depicted below:

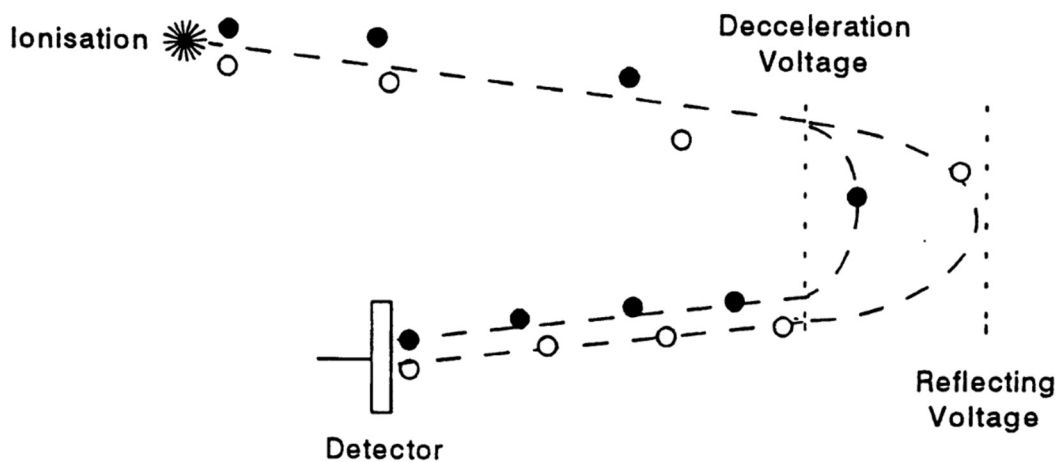


Figure 2.2: Schematic showcasing the basics of the Reflectron¹⁹

All of these advancements in the field of time-of-flight mass spectrometry have led to the technique having widespread usage due to its many advantages. The technique not only has a higher resolution compared to quadrupole and ion-trap mass analyzers, but it's also relatively simple to understand (though admittedly not to maintain), has a high scan speed,

and is applicable to virtually every situation, as it is capable of detecting ions in an extremely large size and mass range²⁰.

Section II: Vacuum Technology

One key ingredient of an operational and successful mass spectrometer is the creation of a high vacuum (10^{-3} - 10^{-9} torr). This is accomplished through a series of vacuum pumps, for which there are many different types to choose from – each serving a very specific purpose. There are three main categories of vacuum pumps: Primary (backing) pumps (also sometimes called roughing pumps, as they create what is known as a “rough” vacuum, which occurs at pressures in between atmospheric pressure and 10^{-4} torr), booster pumps (which for most systems are regarded as optional, but in some cases can be beneficial), and secondary, or high vacuum, pumps.

There are two main categories of roughing pumps: oil-sealed roughing pumps and dry roughing pumps. In these two categories, there are four main types of roughing pumps. The first, a rotary vane pump, the type used in this experiment is an oil-sealed pump where gas is compressed and expelled by a combination of a rotor and vane (hence the name, “rotary vane”) as depicted below:

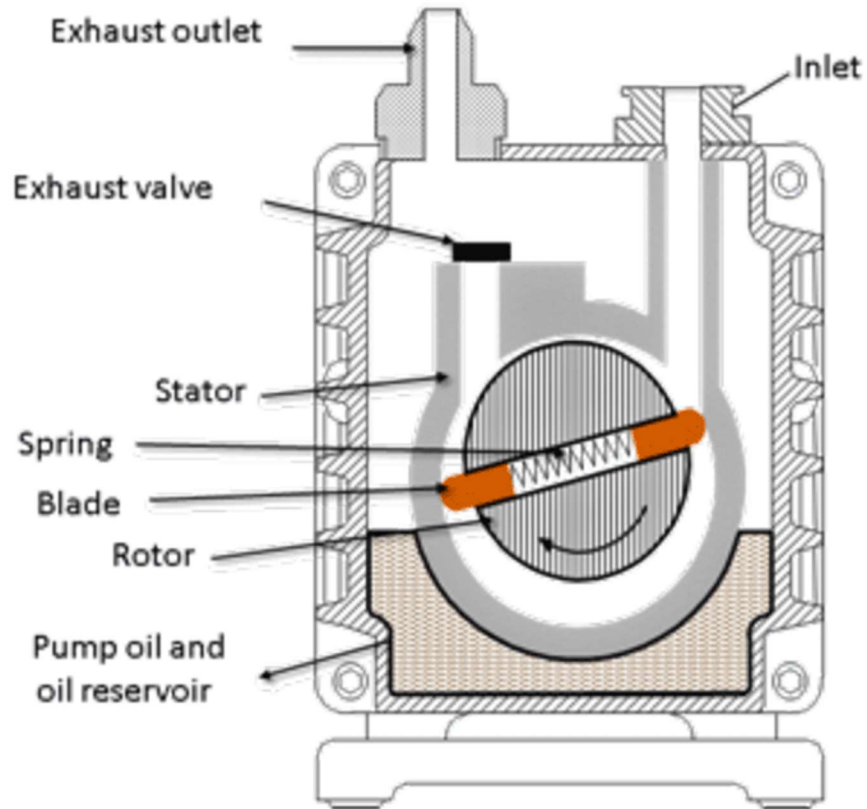


Figure 2.3: Rotary Vane Roughing Pump²¹

The second, a rotary piston pump, is also an oil-sealed pump, except in this model, a piston regulates the suction chamber size as opposed to the vane. The third, known as a roots pump, has to be used in series with either a rotary vane or rotary piston pump, as it cannot work against atmospheric pressure in isolation and allows for hydrocarbon backstreaming. In a roots pump, two rotors, shaped in the form of a figure-eight, spin at increased speeds as compared to their rotary vane and piston counterparts due to their increased separation and the lack of an oil lubricant. However, the lack of operation in isolation makes these pumps less viable in most experimental setups and leads to them sometimes being

classified as booster pumps. The fourth and final type of roughing pump is called a diaphragm pump. A diaphragm pump is a dry roughing pump, meaning it operates without the usage of oil, and unlike roots pumps, it doesn't tolerate hydrocarbon backstreaming. However, while relatively easy to maintain, diaphragm pumps don't reach as high of a vacuum as the other three main types of roughing pumps, so their application is limited²².

After the roughing pumps create the initial rough vacuum, the secondary pumps turn on and create the high vacuum necessary for time-of-flight mass spectrometry. For this purpose, there are again two main categories: kinetic transfer pumps and entrapment pumps. Kinetic transfer pumps transfer the kinetic energy of a rotor or other device to the gas being removed, and entrapment pumps use an electric field and extreme heat to capture gas and remove it²³. Within the kinetic transfer category, there are three main types of vacuum pumps. The first is known as a diffusion pump, which ironically has nothing to do with the actual process of diffusion at all. Instead, a high-speed vapor stream collides with the gas molecules, transferring momentum and kinetic energy upon impact to remove the gas. The second, and the one utilized in this experiment, is known as a turbomolecular pump, where kinetic energy is transferred from incredibly high-speed rotating blades to the gas molecules as depicted below:

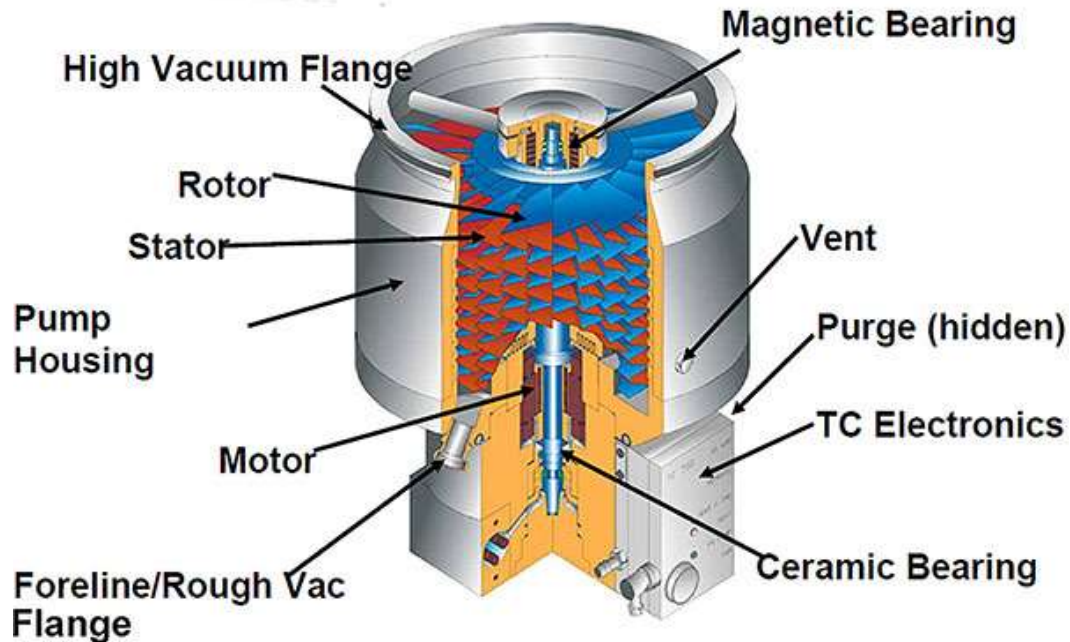


Figure 2.4: Turbomolecular Pump²⁴

The third is called a turbomolecular drag pump, which is similar to a turbomolecular pump but adds a pump drag stage to account for the higher pressure reached by a diaphragm backing pump. A drag stage operates on a similar principle, transporting gas via high-speed rotors, however isn't as sensitive as the main turbomolecular pump and thus can operate at a slightly elevated pressure²².

While for this experiment, the rotary vane and turbomolecular pumps were chosen, it is important to note that no one type of roughing and high-vacuum pump is better than the other. Depending on time, cost, and type of experiment, one slightly less common model could be more useful than the more utilized models.

Chapter III

Experimental Methods

In order to create the dipole-bound anions experimentally, a process known as Rydberg Charge Transfer was utilized. Also called Electron Capture Dissociation or Electron Transfer Dissociation, Rydberg Charge Transfer occurs when electrons attach to a positively charged site on a molecule of gas to create what is known as a hypervalent or Rydberg radical center²⁵. This process can be induced by the experimental setup shown below:

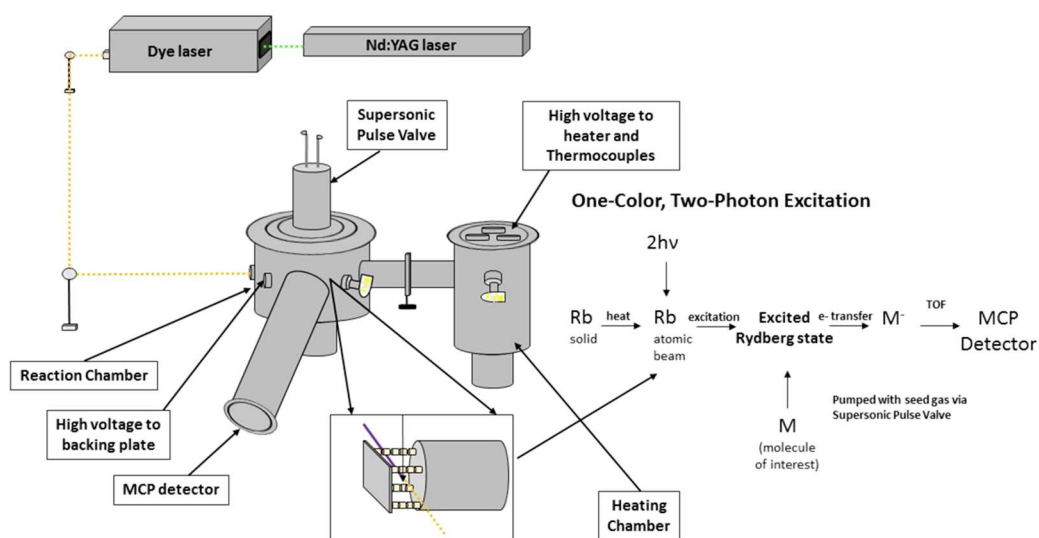


Figure 3.1: Schematic of Experimental Setup²⁶

Before any reaction can occur, a series of roughing and turbomolecular vacuum pumps are used to create a high vacuum (a high vacuum is defined as 1 millitorr to 1 nanotorr, however for this experiment a pressure

of roughly 100 nanotorr was attempted). To accomplish this, two high voltage roughing (or backing) pumps from Marathon Electric and Franklin Electric first brought the pressure in the vacuum chamber down to roughly 8-10 millitorr, and subsequently a series of two turbomolecular vacuum pumps, one a Varian V-250 and the other a Varian V-200, were designed to bring the pressure down to that desired 100 nanotorr or 1×10^{-7} torr. To measure the pressure of the system, a series of different gauges and controllers were utilized. For rough vacuum (down to 100 microtorr), a Granville-Phillips 307 Vacuum Gauge Controller was used to control two convectron gauges (one for each chamber). For high vacuum (100 microtorr to 1 nanotorr), a Granville-Phillips 330 Ionization Gauge Controller was used to control the two MDC Vacuum Products LLC Ionization Gauges. This portion of the experimental setup was the source of many troubles, terrors, and tears, as even once all issues seemed to be resolved, two days later another nearly undiagnosable problem would arise, causing many of the delays in this experiment. It is believed that the vast majority of these issues have been solved, however the validity of this claim remains to be seen.

Once the vacuum is created and all samples inserted (the rubidium into the heating chamber and the molecules under study in a holding chamber on the other side of the supersonic pulsed valve, an Nd:YAG laser (manufactured by Continuum) is pulsed through a dye laser in order to obtain whatever wavelength of light is desired. The beam is then shot

through the reaction chamber to the heating chamber, where the sample of Rubidium atoms is housed. The light excites the electrons in each atom to a higher electronic energy level, and the atoms are then released into the reaction chamber. After a 2 μs reaction, the electron will have transferred to the selected molecule, which is then shot through the Time-of-Flight Mass spectrometer (TOFMS)¹⁰, depicted below:

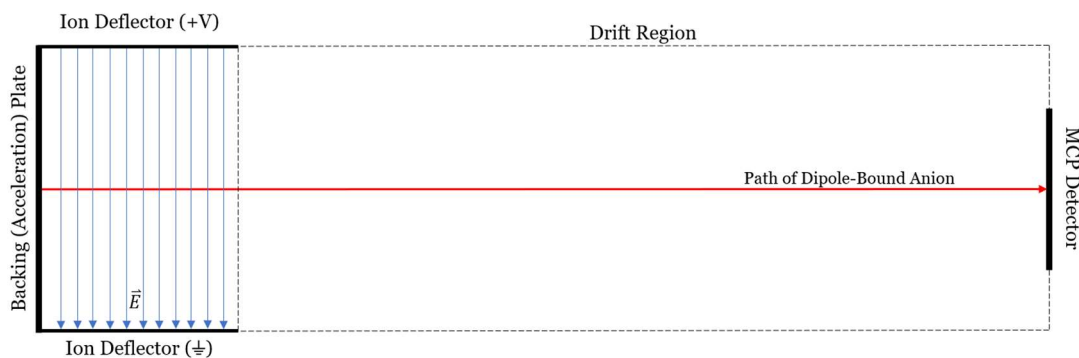


Figure 3.2: Time-of-Flight Mass Spectrometer

TOFMS first accelerates the molecule using an electric field created by the backing plate. Because the dipole-bound anions are negatively charged, ion deflectors (one grounded, one with a positive voltage) are used to alter the path of the anion. Given that the anion would normally drift towards the bottom of the chamber, the electric field shown in Figure 3.1 is used to ensure a straight path so that the anion hits the Multi-Channel Plate (MCP) Detector at the end of the drift chamber. In this experiment, the backing plate and ion deflectors were created using parts from Kimble Physics, and the deflectors were charged using Ortec Model 446 High Voltage Power Supplies. The supersonic pulsed valve that releases the

molecules under study into the reaction chamber is regulated by a BCN Model 8010 Pulse Generator. The custom MCP Detector, based on the following diagram from Delmar Photonics, was previously designed and constructed by previous members of the Hammer Research Group including Dr. Ashley Williams.

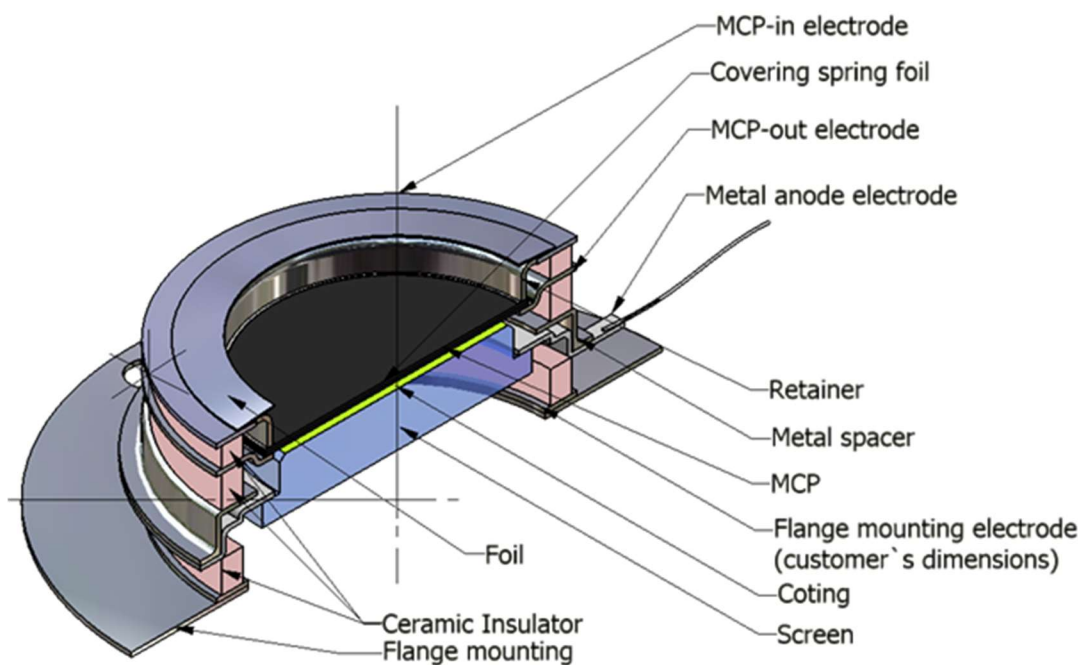


Figure 3.3: Micro-Channel Plate Detector²⁷

In a MCP Detector, when light or a particle hits the first plate, a current is induced by the creation of secondary electrons. This current in turn induces a voltage which can be recorded with an oscilloscope or data acquisition program. For this experiment, the microchannel plates were z-stack mounted, meaning there were three plates mounted parallel to and on top of (with slight spacing in between) one another, as depicted in the figure below

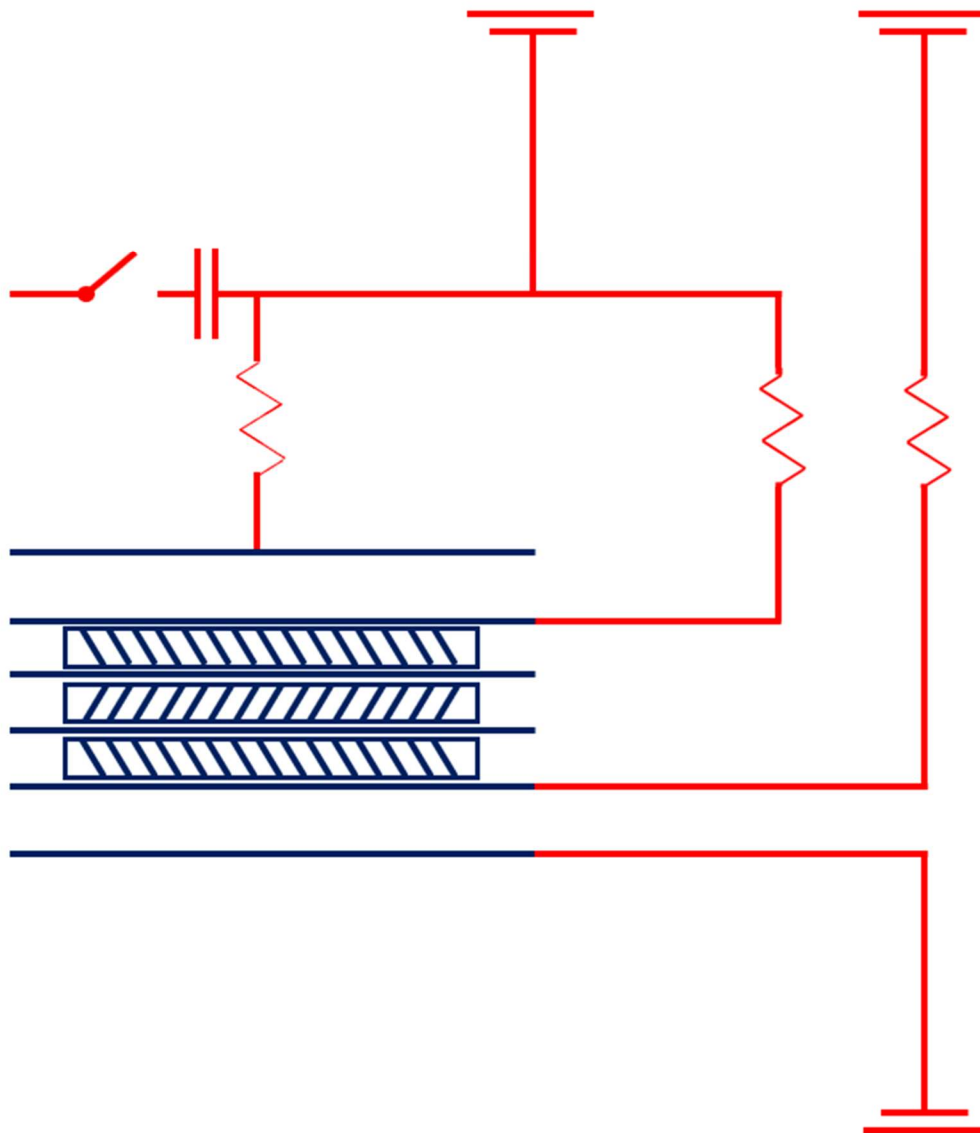


Figure 3.4: Z-Stack Mounted Micro-Channel Plate Detector

From the time it takes to reach the detector as well as the distance of 69 centimeters between the edge of the deflector and the detector, the velocity, and thus acceleration, of the anions can be calculated. The mass of the anions, and thus their identity, can then finally be found via the following differential equation¹⁰:

$$m\ddot{x} = e\vec{E}$$

which when doubly integrated yields the following formula for time³:

$$t = \sqrt{\frac{2mx}{eE}}$$

where m is the mass of the anion, x is the length of the mass spectrometer, e is the unit charge of an electron (and also the charge of our dipole-bound anions), and E is the electric field strength.

Chapter IV

Computational Chemistry

Section I: Introduction to Quantum Chemistry

Quantum Mechanics was the burgeoning scientific field of the early 20th Century. While the details of quantum theory were and, to an extent, still are debated extensively, Austrian Physicist Erwin Schrödinger developed in 1926 what has been named The Schrödinger Equation²⁸, which is of the form

$$\hat{H}\psi = E\psi$$

a formula to find the energy of a particle, E, from solving the eigenvalue problem presented when the Hamiltonian operator, \hat{H} , acts on the particles wave equation, given by ψ . Now, the Hamiltonian is made up of five components: the electron kinetic energy (\hat{T}_e), the nuclear kinetic energy (\hat{T}_n), the nuclear-nuclear repulsion (\hat{V}_{nn}), the nuclear-electronic attraction (\hat{V}_{ne}), and the electron-electron repulsion (\hat{V}_{ee}). Thus, our Hamiltonian in its full form is²⁹

$$\hat{H} = \hat{T}_e + \hat{T}_n + \hat{V}_{ne} + \hat{V}_{ee} + \hat{V}_{nn}$$

Now, the Hamiltonian is perfectly solvable for the hydrogen atom. Even without using computational methods or any approximations, the wavefunction ψ for hydrogen can be found. However, it is this last term in the Hamiltonian, the electron-electron repulsion, that makes every single

other atom on the periodic table *impossible* to solve. Due to the fact that electrons are *always* in motion and their precise location can never truly be determined, we can never know the exact amount of repulsion that is taking place. Thus, in order to solve Schrödinger's Equation, we need approximations and computational methods. The first approximation is known as the Born-Oppenheimer Approximation, which assumes that the nuclear and electronic motions, and thus kinetic energies, are separate, and that since \hat{T}_n is vastly smaller than \hat{T}_e , it can be neglected, treating the nuclei as fixed point masses. Our Hamiltonian then becomes

$$\hat{H} = \hat{T}_e + \hat{V}_{ne} + \hat{V}_{ee} + \hat{V}_{nn}$$

where V_{nn} is a constant since the nuclei are fixed in place. Next, with the introduction of Hartree-Fock Theory, close approximations for the electron's wavefunction and total energy can be found. In Hartree-Fock Theory, instead of attempting to find the true correlation of the two electrons (which in computational chemistry is known as the Full Configuration Interaction (FCI) Limit), the two electrons are treated as one moving point mass and a "cloud" of electron density. The correlation between the single electron and each point in the cloud is determined, and these are all then integrated together to create a decent approximation for the true correlation. First, an initial "guess" for the electron's wavefunction is made, and then after solving the eigenvalue equation for E , a new wavefunction is also obtained, which is then reinserted back into the eigenvalue equation as the new eigenfunction. This step is performed

iteratively until energy is minimized and matches that which we can derive experimentally. The initial guess for the wavefunction is of the form

$$\Psi_{HP}(\mathbf{r}_1, \mathbf{r}_2, \dots, \mathbf{r}_N) = \varphi_1(\mathbf{r}_1)\varphi_2(\mathbf{r}_2) \dots \varphi_N(\mathbf{r}_N)$$

and is known as the Hartree Product²⁸. Now, this equation is merely a representation of spatial orbitals, which do not satisfy the requirement that wavefunctions describing fermions must satisfy the antisymmetry principle, so spin orbitals must be used. These are represented by

$$\Psi_{HP}(\mathbf{x}_1, \mathbf{x}_2, \dots, \mathbf{x}_N) = \chi_1(\mathbf{x}_1)\chi_2(\mathbf{x}_2) \dots \chi_N(\mathbf{x}_N)$$

where $\chi(\mathbf{x})$ is a spin orbital, and $\mathbf{x} = \{\mathbf{r}, \omega\}$, where ω is the spin coordinate. The spin coordinate can be either α or β , where β is simply not α and vice versa. Now, this formula is only antisymmetric in special cases, so the initial guess for the Hartree-Fock approximation for a two-electron problem must be generally represented as the normalized wavefunction

$$\Psi(\mathbf{x}_1, \mathbf{x}_2) = \frac{1}{\sqrt{2}}[\chi_1(\mathbf{x}_1)\chi_2(\mathbf{x}_2) - \chi_1(\mathbf{x}_2)\chi_2(\mathbf{x}_1)]$$

This can also be written in matrix representation, which can be expanded to give the solution for multi-electron problems with 3 or more electrons, known as a Slater Determinant, as shown by the following equation³⁰

$$\Psi(\mathbf{x}_1, \mathbf{x}_2, \dots, \mathbf{x}_N) = \frac{1}{\sqrt{2}} \begin{vmatrix} \chi_1(\mathbf{x}_1) & \chi_2(\mathbf{x}_1) & \dots & \chi_N(\mathbf{x}_1) \\ \chi_2(\mathbf{x}_1) & \chi_2(\mathbf{x}_2) & \dots & \dots \\ \dots & \dots & \dots & \dots \\ \chi_N(\mathbf{x}_1) & \dots & \dots & \chi_N(\mathbf{x}_N) \end{vmatrix}$$

This is then inserted into the Schrödinger Equation to obtain the energy, and the coefficients of each piece are subsequently changed to find the wavefunction that minimizes the total energy of the system. Once this occurs, the calculation is complete, and the “true” wavefunction and energy are obtained. Hartree Fock Theory, however, is merely the beginning of Computational Chemistry. Beyond Hartree Fock, perturbative methods such as MP2, Coupled Cluster Theory, and even Density Functional Theory (e.g. B3LYP), all attempt to solve this two-electron correlation problem. CCSD(T) (Coupled Clusters Singles Doubles (Triples)), is currently considered the “gold standard” for performing computational work, however new methods are currently being designed and tested every day – all attempting to get closer and closer to that FCI Limit.

Section II: Computational Methods

Hartree Fock Theory formed the basis of my computational study of multipole-bound anions, where I performed MP2- and CCSD-level calculations in the Gaussian 16 Software Package to determine the dipole moments and electron affinities of six molecules in question. These six were chosen due to their extremely high dipole moment and the presence of either Nitrogen or Sulfur (with the exception of Furfural, which I chose solely due to its high dipole moment and pure intrigue). These six molecules were 1,3-Dioxolan-2-thione, 1,3-Dioxole-2-thione, Ethylene-thiocarbonate, Vinylene-thiocarbonate, 1,3,4-Thiadiazole, and, as

previously mentioned, Furfural. For each molecule, the initial geometry was obtained using Gaussview 6.0, with the initial geometry optimization being performed using the Hartree Fock method and aug-cc-pvdz basis set. After performing this basic geometry optimization, I proceeded to add additional molecular orbitals to each molecule as shown by the example input file for ethylene-thiocarbonate below:

```
%chk=ecopt.chk
%mem=2000MB
%nprocs=2
# mp2/aug-cc-pvdz extrabasis guess=read nosymm
```

EC orbitals

```
O 1
C   -0.000216  -0.168461  -0.226105
S   -0.220032   1.589081  -0.274460
S    0.219718  -0.812550   1.409865
S   -0.000429  -1.114747  -1.575331
C    0.262407   1.894741   1.467273
C   -0.262280   0.721045   2.290538
H    1.359489   1.965331   1.527883
H   -0.194126   2.846317   1.783019
H   -1.359338   0.754165   2.377794
H    0.194469   0.693767   3.292661
```

H 0

S 1

0.0025 1.0

P 1

0.01 1.0

S 1

0.00025 1.0

P 1

0.001 1.0

```

S 1
0.000025 1.0
P 1
0.0001 1.0
S 1
0.00005 1.0
P 1
0.00001 1.0
S 1
0.000025 1.0
****
C o
SP 1
0.005475 1.0 1.0
D 1
0.07825 1.0
****

```

In adding these additional orbitals (the values for which came from the Basis Set Exchange³¹), it was possible to find the electron affinity of the molecule, or in other words, how much energy is utilized in electrostatically binding that excess electron to create the multipole- (or in the case of all six of these molecules, dipole-) bound anions. This is possible even without changing the charge and multiplicity of the molecule thanks to the principles outlined in Koopman's Theorem, which states that "the first ionization energy of a molecule is equal to the negative of the energy of the highest occupied molecular orbital."³² This initial theorem has been further generalized to show that the electron affinity of a molecule is equivalent to the energy of the lowest unoccupied molecular orbital. The higher the energy, the more tightly bound the electron and thus more stable the molecular ion is. Each orbital was added sequentially,

meaning an initial geometry optimization was performed, followed by the addition of the first orbital (for this input file, the lines H O/S 1/0.0025 1.0 were added) and subsequently the remaining orbitals (along with the keyword guess=read in order to use the optimizations from the checkpoint file) until no change in the first virtual eigenvalue was detected. After performing these calculations at the MP2 and CCSD level, dipole moments of each molecule were calculated (in order to prove consonance with literature values), using the MP2 level of theory and the command “density=current.”

Chapter V

Results

Due to an unforeseen and large of issues and setbacks, there are no experimental results for this project as of this writing. The experimental portion of this project is projected to be complete by the end of the Summer of 2022. That being said, the computational results are promising and predict an interesting and successful experiment once all issues with the experimental setup are resolved. As stated previously, the six molecules under study were chosen due to their extremely high dipole moments as reported in the literature³³, which were confirmed with a simple dipole moment calculation detailed previously using the same method and basis set as the calculation for the Electron Affinity in order to provide a more precise comparison. While the calculated values for the dipole moment (all in Debye) may not be *exactly* what was reported via prior experiments, performing these calculations in the same manner as all others eliminates any discrepancies in level of theory or basis set size that would cause illegitimate comparison. However, since these values are *close* to their ancient experimental counterparts, the newly calculated values for the electron affinities of each molecule are also most likely accurate. As is shown in Table 5.1 and Figure 5.1, depicted below, in the six molecules under study, an increase in dipole moment is correlated with an increase in electron affinity:

Table 5.1: Calculated Dipole Moments and Electron Affinities of Selected Molecules

Molecule	Dipole Moment (Debye)	Electron Affinity (meV)
1,3,-Dioxolan-2-thione	5.5860	44.9
1,3,-Dioxole-2-thione	4.8960	25.03
Ethylene-trithiocarbonate	4.8199	16.33
Vinylene-trithiocarbonate	4.5364	8.44
Furfural	4.0577	2.45
1,3,4-Thiadiazole	3.5416	0.27

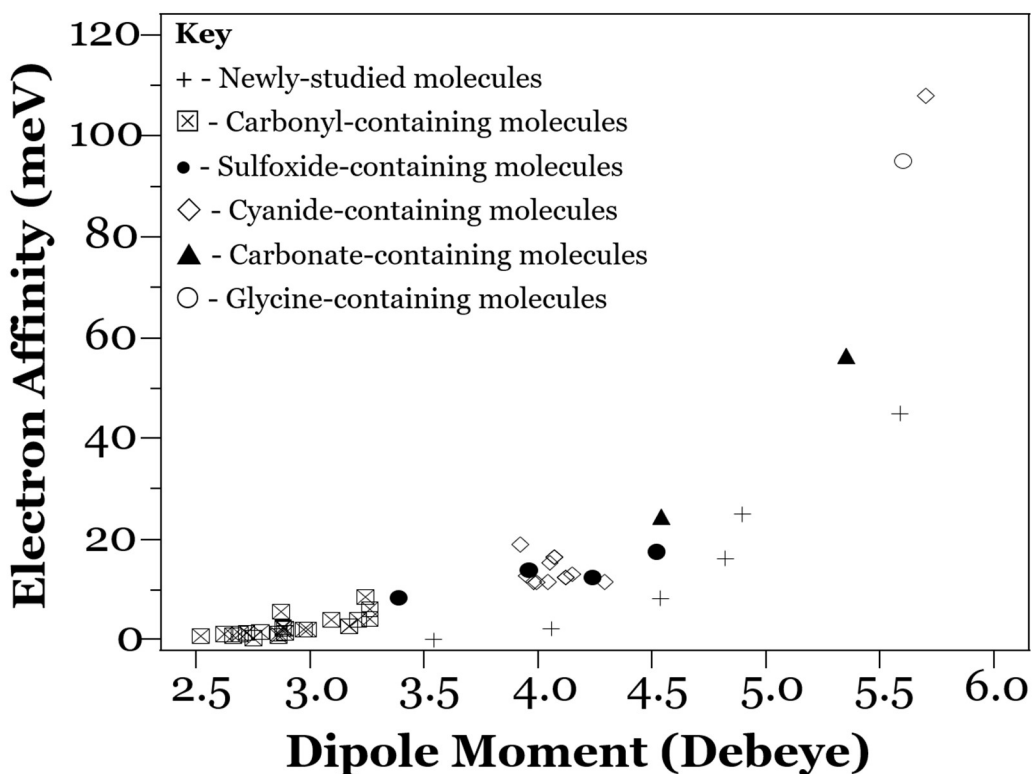


Figure 5.1: Comparison of Dipole Moments and Electron Affinities of New Molecules with Previously-Studied Molecules^{10,12-13}

Due to the fact that the excess electron is bounded due to the electron deficit on the positively charged side of the molecule, this result correlates with the underlying hypothesis of the experiment – that a molecule with an extremely high dipole moment due to the presence of either a nitrogen or sulfur atom will electrostatically bind an excess electron. As previously stated in Chapter 4, the molecule with the largest electron affinity, and from these results the largest dipole moment, will be the strongest and thus most stable multiple-bound anion. It is seen via these tables and figures that 1,3-dioxolan-2-thione is the best candidate for experimental study, while 1,3,4-Thiadiazole is the weakest candidate presented in this

thesis. However, the mere *existence* of a dipole-bound state, however weak it may be, is enough to show that 1,3,4-Thiadiazole is worthy of experimental testing. Furthermore, Figure 5.2 shows the optimized Lowest Unoccupied Molecular Orbitals for each molecule (i.e. where the electron would electrostatically bind), all of which, including that of 1,3,4-Thiadiazole, appear very similar in nature aside from the strengths provided in Table 5.1.

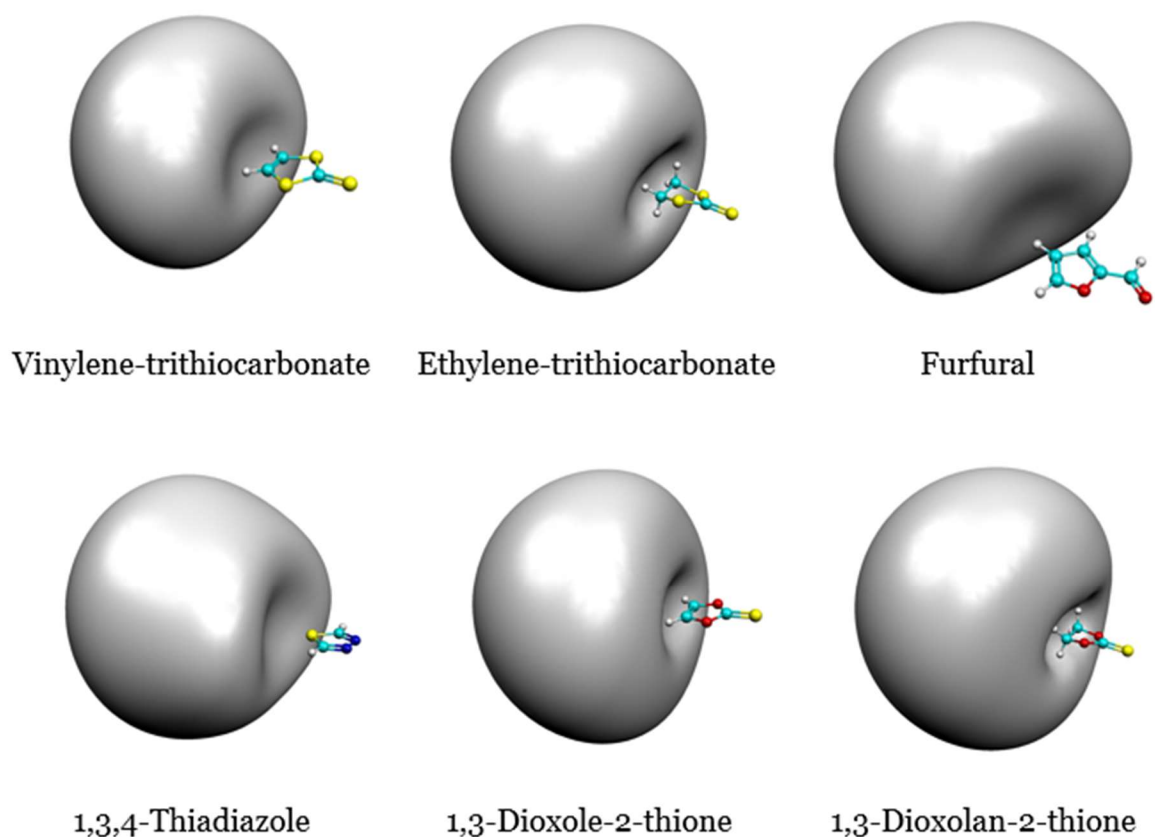


Figure 5.2: Optimized Lowest Unoccupied Molecular Orbitals

However, it can be seen in this figure that the LUMO for 1,3,4-Thiadiazole has one differentiating factor from its five counterparts. All LUMO orbitals

for the other five (for which the electron affinity is greater by tenfold or more) are centrally located around at least one hydrogen atom, while the LUMO for 1,3,4-Thiadiazole is located around the sulfur atom. As shown in Chapter IV, the hydrogen atoms were the first and main candidate for extra basis functions, meaning that this increased distance from atom to orbital could possibly be the cause for the discrepancy in electron affinity. Applying this same logic to the remaining five molecules, it becomes apparent that an increase in the number of hydrogen atoms located near the LUMO in addition to the presence of highly-electronegative atoms is most likely the cause for an increase in molecular electron affinity. In comparing the two highest electron affinity values, 44.9 meV for 1,3,-Dioxolan-2-thione and 25.03 meV for 1,3,-Dioxole-2-thione, it can be seen in Figure 5.2 that 1,3,-Dioxolan-2-thione contains a carbon-carbon single bond and *four* hydrogen atoms near the LUMO whereas 1,3,-Dioxole-2-thione contains a carbon-carbon double bond and thus only *two* hydrogen atoms. Additionally, the optimized structure shows an almost planar conformation for 1,3,-Dioxole-2-thione and a non-planar conformation for 1,3,-Dioxolan-2-thione. Likewise, the principal difference between these two molecules and their counterparts ethylene-trithiocarbonate and vinylene-trithiocarbonate is the presence of two oxygen atoms. Given that the two pairs follow a similar pattern with regards to carbon-carbon bond type, hydrogen atom count, and geometry, its most likely that the cause for the increase in electron affinity values for 1,3,-Dioxolan-2-thione and 1,3,-Dioxole-2-thione is the increased electronegativity of oxygen as compared

to sulfur. This could also explain the discrepancy in electron affinity values between furfural and 1,3,4-thiadiazole and between these two molecules and the other four. The increased electronegativity of oxygen compared to nitrogen could be the cause for the higher EA value for furfural, and the increase in electronegative atom count (two oxygen atoms on furfural versus this plus an additional sulfur atom in 1,3,-Dioxolan-2-thione) is likely the cause for the lower EA value for furfural as compared to the trithiocarbonates and dioxoles.

Comparing the electron affinities of these six molecules with those previously studied, a deviation from the previous trend can be seen. This is most likely due to the fact that the EA values for the vast majority of molecules previously studied by other research groups (as opposed to those studied by Dr. Ashley Williams and myself) were found experimentally, whereas ours were found computationally. Additionally, while higher levels of theory (CCSD versus MP2) did reveal the same result in the current study, it is possible that an even larger basis set (such as the augmented coupled-cluster quadruple zeta basis set, aug-cc-pvqz) or even better method (such as the “gold standard,” CCSD(T)), would result in EA values that fit the current trend more closely.

Chapter VI

Conclusions and Future Work

The computational results presented in this thesis show that the six molecules studied are excellent candidates for experimental study and therefore could be pivotal in advancing the understanding of electron transport processes in dye-sensitized solar cells. Once these processes are more thoroughly understood, more efficient light harvesting through the optimization of their structures could become a reality. Knowing that an increase in dipole moment corresponds with an increase in molecular electron affinity, future candidates for experimental study could potentially be chosen based upon dipole moment alone if the computational expense outweighs its utility. As for these six, Table 5.1 shows that 1,3-dioxolan-2-thione promises to be the easiest dipole-bound anion to create experimentally, whereas 1,3,4-thiadiazole could present the most challenges. It was also found that the increase in electron affinity is correlated with the number of hydrogen atoms surrounding the lowest unoccupied molecular orbital as well as the number and identity of electronegative atoms or electron withdrawing groups in the molecule.

To continue this exciting project, a finalized experimental setup will be necessary in which all issues regarding vacuum technology are resolved and the components redesigned for this thesis are confirmed to be operational and optimized. Once completed, the experimental setup described earlier will confirm the existence of these molecules, the

properties of which can be better understood with further computational studies. To better understand the electron transport processes, a subsequent computational study involving higher levels of theory and larger basis sets would be necessary. Finally, the comparison of these six molecules to structurally similar molecules could prove the reasons presented previously explaining the discrepancies in electron affinity and dipole moment. Performing computational and possibly experimental studies on molecules with, for example, an additional hydrogen atom, an additional electron withdrawing group, or a different electron withdrawing group could help further explain why these six molecules present so much potential in understanding electron transport processes in dye-sensitized solar cells.

Chapter VII

References

1. B. O'Regan, M. Grätzel, *Nature*, 353 (1991), p. 737
2. Brogdon, P., L. E. McNamara, et al. (2016). "Toward tightly bound carboxylic acid-based organic dyes for DSCs: relative TiO₂ binding strengths of benzoic acid, cyanoacrylic acid, and conjugated double carboxylic acid anchoring dyes." *Synthetic Metals* 222: 66-75.
3. Chandan, R., A. Prabhakar, et al. (2019). 8 - Stimuli-responsive polymers for image-guided therapeutic applications. *Stimuli Responsive Polymeric Nanocarriers for Drug Delivery Applications*. A. S. H. Makhoulouf and N. Y. Abu-Thabit, Woodhead Publishing: 219-245.
4. Snaith, H. J. (2010). "Estimating the Maximum Attainable Efficiency in Dye-Sensitized Solar Cells." *Advanced Functional Materials* 20(1): 13-19.
5. Nugegoda, D., L. A. Hunt, et al. (2022). "Lewis Acid–Lewis Base Interactions Promote Fast Interfacial Electron Transfers with a Pyridine-Based Donor Dye in Dye-Sensitized Solar Cells." *ACS Applied Energy Materials* 5(2): 1516-1527.
6. Cheema, H., A. Baumann, et al. (2019). "Near-Infrared-Absorbing Indolizine-Porphyrin Push–Pull Dye for Dye-Sensitized Solar Cells." *ACS Applied Materials & Interfaces* 11(18): 16474-16489.
7. Zhang, Y., H. Cheema, et al. (2018). "Ullazine Donor– π bridge-Acceptor Organic Dyes for Dye-Sensitized Solar Cells." *Chemistry – A European Journal* 24(22): 5939-5949.

8. Cheema, H., A. Peddapuram, et al. (2017). "Molecular Engineering of Near Infrared Absorbing Thienopyrazine Double Donor Double Acceptor Organic Dyes for Dye-Sensitized Solar Cells." *The Journal of Organic Chemistry* 82(23): 12038-12049.
9. Zito, B. B. (2022, March 3). Here are the most efficient types of solar panels. *Forbes*. Retrieved May 5, 2022, from <https://www.forbes.com/advisor/home-improvement/most-efficient-solar-panels/>
10. Hammer, Nathanael Isaac, "Dipole-Bound Anions. " PhD diss., University of Tennessee, 2003. https://trace.tennessee.edu/utk_graddiss/2065
11. Costa Filho, R. N., G. Alencar, et al. (2013). "Morse potential derived from first principles." *EPL (Europhysics Letters)* 101(1): 10009.
12. Hammer, N. I., K. Diri, et al. (2003). "Dipole-bound anions of carbonyl, nitrile, and sulfoxide containing molecules." *The Journal of Chemical Physics* 119(7): 3650-3660.
13. Hammer, N. I., R. J. Hinde, et al. (2004). "Dipole-bound anions of highly polar molecules: Ethylene carbonate and vinylene carbonate." *The Journal of Chemical Physics* 120(2): 685-690.
14. Desfrancois, C., Y. Bouteiller, et al. (2004). "Long-Range Electron Binding to Quadrupolar Molecules." *Physical Review Letters* 92(8): 083003.
15. Diken, E. G., N. I. Hammer, et al. (2004). "Preparation and photoelectron spectrum of the glycine molecular anion: Assignment to a dipole-bound electron species with a high-dipole moment, non-zwitterionic form of the neutral core." *The Journal of Chemical Physics* 120(21): 9899-9902.

16. E. Fermi and E. Teller, Phys. Rev. 72, 406 (1947).
17. R. F. Wallis, R. Herman, and H. W. Milnes, J. Mol. Spectrosc. 4, 51 (1960)
18. Hendricks, J. H., H. L. De Clercq, et al. (1997). "Negative ion photoelectron spectroscopy of the ground state, dipole-bound dimeric anion, (HF)₂." The Journal of Chemical Physics 107(8): 2962-2967.
19. Price, D. (1993). Time-of-Flight Mass Spectrometry. Time-of-Flight Mass Spectrometry, American Chemical Society. 549: 1-15.
20. Kaklamanos, G., E. Aprea, et al. (2016). Mass Spectrometry: Principles and Instrumentation. Encyclopedia of Food and Health. B. Caballero, P. M. Finglas and F. Toldrá. Oxford, Academic Press: 661-668.
21. International, V. A. C. A. E. R. O. (2019, December 10). An introduction to vacuum pumps. Vacaero. Retrieved May 5, 2022, from <https://vacaero.com/information-resources/vacuum-pump-technology-education-and-training/1039-an-introduction-to-vacuum-pumps.html>
22. Gatzen, H. H., Saile, V., & Leuthold Jürg. (2016). Micro and nano fabrication tools and Processes. Springer Berlin.
23. Watanabe, F. and A. Kasai (1999). "Entrapment pump: Noble gas pump for use in combination with a getter pump." Journal of Vacuum Science & Technology A 17(5): 3103-3107.
24. Kurt J. Lesker Company. (n.d.). Kurt J. Lesker company. Kurt J. Lesker Company. Retrieved May 5, 2022, from <https://www.lesker.com/newweb/faqs/question.cfm?id=477>

25. Sobczyk, M. and J. Simons (2006). "The Role of Excited Rydberg States in Electron Transfer Dissociation." *The Journal of Physical Chemistry B* 110(14): 7519-7527.
26. Williams, Ashley E., "A Spectroscopic and Quantum Chemical Investigation into the Hydrogen Bonding and Charge Accommodation of Biomolecules and their Building Blocks in Various Environments" (2021). Electronic Theses and Dissertations.
27. Del-Mar Photonics. (n.d.). Microchannel Plates. Microchannel plates. Retrieved May 5, 2022, from http://www.dmp Photonics.com/MCP_MCPImageIntensifiers/microchannel_plates.htm
28. The Nobel Prize. (n.d.). The nobel prize in physics 1933. NobelPrize.org. Retrieved May 5, 2022, from <https://www.nobelprize.org/prizes/physics/1933/schrodinger/biographical/>
29. Szabo, A., & Ostlund, N. S. (2020). *Modern quantum chemistry introduction to advanced electronic structure theory*. Dover Publications, Inc.
30. Sherrill, D. C., *An Introduction to Hartree-Fock Molecular Orbital Theory*. Georgia Institute of Technology: School of Chemistry and Biochemistry, 2000.
31. Basis Set Exchange. (n.d.). Basis Set Exchange (BSE). Basis Set Exchange. Retrieved May 5, 2022, from <https://www.basissetexchange.org/>

32. Libretexts. (2020, August 15). Koopmans' theorem. Chemistry LibreTexts.

Retrieved May 5, 2022, from

[https://chem.libretexts.org/Bookshelves/Physical and Theoretical Chemistry Textbook Maps/Supplemental Modules \(Physical and Theoretical Chemistry\)/Quantum Mechanics/10%3A Multi-electron Atoms/Koopmans%27 Theorem](https://chem.libretexts.org/Bookshelves/Physical_and_Theoretical_Chemistry_Textbook_Maps/Supplemental_Modules_(Physical_and_Theoretical_Chemistry)/Quantum_Mechanics/10%3A_Multi-electron_Atoms/Koopmans%27_Theorem)

33. NIST Chemistry Webbook. (n.d.). Experimental dipoles. CCCBDB list of

experimental dipole moments. Retrieved May 5, 2022, from

<https://cccbdb.nist.gov/diplistx.asp#1971Whi/Bog:4714-4717>